Adsorption (2015) 21:533–546
DOI 10.1007/s10450-015-9692-6

DFT analysis of coordination polymer ligands: unraveling the electrostatic properties and their effect on CO_2 interaction

Paul J. Meza-Morales[1] · Alberto Santana-Vargas[2] · María C. Curet-Arana[1]

Received: 17 February 2015 / Revised: 27 July 2015 / Accepted: 14 September 2015 / Published online: 21 September 2015

Abstract Coordination polymer with pillared layer structures, also known as coordination polymer ligands (CPLs) are a novel class of nanoporous adsorbent materials that exhibit higher adsorption affinity for CO_2 than for other small molecules, such as O_2, N_2, and CH_4. In this work, DFT calculations were used to analyze the relation between electrostatic properties of CPL-2, CPL-4, CPL-5, and CPL-7, and their interaction with CO_2, in order to elucidate structural features that promote this interaction. The B3LYP and ωB97XD functionals were used to calculate electrostatic properties, including atomic charges, electrostatic potential, electric field, and electric field gradient. Both functionals showed similar results and indicated that the pore exposed carboxylate groups in each CPL-n have a strong charge separation, a mixed electrostatic potential, and a high electric field gradient. In general, three CO_2 interacting regions were elucidated. The principal interacting sites are the pore exposed carboxylate groups, the aromatic ring from pyrazine-2,3-dicarboxylate (*pzdc*) groups, and some chemical functionalities at the pillar-ligands. The CO_2 electrostatic potential upon interaction revealed that the interaction is dictated by the coupling of the electrostatic potential between the CO_2 and the CPL-n model.

Keywords Coordination polymer ligands · Density functional theory · CO_2 interaction · Electrostatic properties

1 Introduction

In the last two decades, much effort has been put forth in finding adsorbent materials to remove CO_2 selectively (Kuppler et al. 2009; Li et al. 2009, 2011, 2012; Millward and Yaghi 2005; Rezakazemi et al. 2014; Songolzadeh et al. 2012; Sumida et al. 2012; Uribe-romo et al. 2010; Yu 2012). An adequate adsorbent material for CO_2 storage and delivery must fulfill a series of technical requirements, such as large adsorption capacity, adsorption selectivity, regenerability, thermal stability, and low volume/pressure gas storage ratio (Bae and Snurr 2011; Choi et al. 2009). In the late 1990s, Kitagawa and co-workers developed a novel class of nanoporous adsorbent materials known as coordination polymer with pillared layer structures or coordination polymer ligands (CPLs), which belong to porous coordination polymers (PCPs) family (Kitagawa et al. 2004; Kondo et al. 1999; Noro et al. 2000). The CPLs consist of 2D neutral layers formed by Cu^{2+} ions and the ionic pyrazine-2,3-dicarboxylate (*pzdc*), and the layers are separated by an organic pillar ligand, as shown in Fig. 1. This arrangement results in pore channels extended in 1D. Recently, Hernández-Maldonado and co-workers carried out systematic adsorption experiments, and they demonstrated that CPLs, including CPL-2, CPL-4, CPL-5, CPL-6, and CPL-7, exhibited higher adsorption affinity for CO_2 than for other small molecules, such as O_2, N_2, and CH_4

Electronic supplementary material The online version of this article (doi:10.1007/s10450-015-9692-6) contains supplementary material, which is available to authorized users.

✉ María C. Curet-Arana
maria.curetarana@upr.edu

[1] Department of Chemical Engineering, University of Puerto Rico - Mayaguez Campus, Road 108 - km 1.1, Call Box 9000, Mayaguez, PR 00681-9000, USA

[2] Department of Chemistry, University of Puerto Rico - Mayaguez Campus, Road 108 - km 1.1, Mayaguez, PR 00681-9000, USA

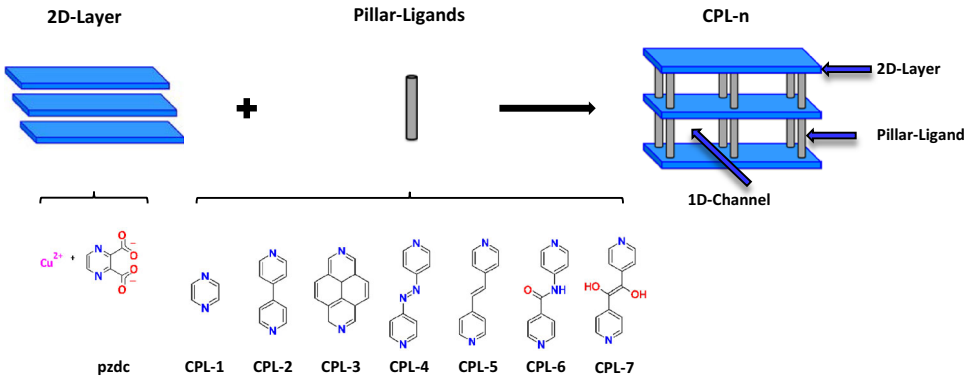

Fig. 1 Schematic representation of the CPL-n with different linkers ligands used as pillars. *pzdc* 2,3-pyrazinedicarboxylate, *CPL-1* 1,4′-pyrazine (*pyz*), *CPL-2* 4,4′-bipyridyl (*bipy*), *CPL-3* 2,7-diazapyrene (*dap*), *CPL-4* 4,4-azopyridine (*abp*), *CPL-5* 1,2-(4-pyridyl) ethylene (*bpe*), *CPL-6* 4-pyridinecarboxamide (*pin*), and *CPL-7* 1,2-di(4-pyridyl)-(glycol) (*bpyg*)

(García-Ricard et al. 2011, 2012, 2013; García-Ricard and Hernández-Maldonado 2010). They concluded that the sustained delivery of CO_2 at moderate pressure range, the fully reversible CO_2 adsorption isotherms of some of these CPLs, and the low CO_2 isosteric heat of adsorption, which ranged in the physical adsorption range, make CPLs an attractive alternative for the selective CO_2 adsorption applications.

In order to design new adsorption materials with higher selectivities and adsorption capacities than the current technologies, it is necessary to understand the underlying interaction between CO_2 and the adsorbent material frameworks. One of the main challenges for gas separation materials is that, in most cases, the differences in the properties of the gases that have to be separated are relatively small. For example, the size, shape and the kinetic diameter of CO_2 are not that different to those of O_2, N_2, H_2O or CH_4 (Bae et al. 2004). Differences, however, are more noticeable when comparing the electronic properties, such as valence electron configuration, electron density, electric multipole moments and polarization. Therefore, materials for the efficient capture of CO_2 require a molecular level of control that can take advantage of differences in the electronic properties of the gas molecules. Computational chemistry methods, such as density functional theory (DFT) methods have become ideal alternatives for screening new possible adsorption materials. These techniques provide valuable information including partial atomic charges, electronic configurations, and even electric and magnetic properties at low computational cost.

Several experimental and theoretical works have explored the molecular properties related to the adsorption of CO_2, which included quadrupole moment, polarizability, and electrostatic potential (Glaser et al. 2000, 2002; Harries 1970; Haskopoulos and Maroulis 2006; Lewis et al. 2000; Maroulis 2003, 2004; Varanasi 1970). For example, Noro and co-workers used DFT calculations to analyze a CO_2-Cu based PCP system (Noro et al. 2013). They found that the inclusion of inorganic fluorinate PF_6^- anions in the framework decrease the interaction energy, hence improving not only the selectivity for CO_2 but also the regenerability process. Culp and co-workers used DFT calculations to analyze the interaction between CO_2 and a Fe-based PCP system (Culp et al. 2013). They observed that the spin state of the PCP has an impact on the CO_2 interaction energy, the interacting site, and the arrangement of CO_2 within the pore structure. Deshmukh and co-workers used a combination of MP, DFT, and HF calculations to analyze a Hofmann-type PCP (Deshmukh et al. 2013). In their work, they performed a decomposition energy analysis and quantified the influence of the electrostatic and dispersion contributions to the interaction energy for CO_2 and CS_2 molecules. They found that the orientation of the CO_2 within the pores is stabilized by electrostatic interactions, while for CS_2, the orientation is stabilized by dispersion interactions. Hijikata and Sakaki also used a combination of MP, DFT, and HF calculation to analyze the interaction of several small molecules, including CO_2, on a Cu paddle-wheel units (Hijikata and Sakaki 2014). They also used a decomposition energy analysis, and they found a linear positive relation between the interaction energy and the electrostatic contribution, and a linear negative relation for the interaction energy and the exchange–correlation contribution. Other publications (Li et al. 2011, 2012 and Ji et al. 2014) provide comprehensive summaries of quantum mechanical calculation of similar type of adsorbent materials.

Most of the published work involving quantum mechanical calculations for the analysis of CO_2 and adsorbent materials are focused on elucidating interacting sites, calculating interaction energies, and performing energy decomposition analysis (Grajciar et al. 2011, 2015; Liu et al. 2012; Nijem et al. 2011; Pianwanit et al. 2008; Ramsahye et al. 2008; Vaidhyanathan et al. 2010; Yu and Balbuena 2013; Zhou et al. 2011). However, the electrostatic properties of the adsorbent materials in most cases still remain unclear. In this work, systematic DFT calculations were used to elucidate the electrostatic properties of

four CPL-n materials, including atomic charges, electrostatic potential, electric field, and electric field gradient. We have also performed a systematic analysis of the interaction between CO_2 and various CPL-n. These sets of calculations have allowed us to identify electrostatic properties that promote CO_2 interactions.

2 Methodology

2.1 Models

Four CPL-n (CPL-2, CPL-4, CPL-5, and CPL-7), were studied in this work. For each CPL-n, a simplified cluster model was created from the reported crystallographic data (Kitaura et al. 2002; Matsuda et al. 2010; Sakamoto et al. 2010; Uemura et al. 2006). In our calculations, it was assumed that the adsorbent materials were fully activated, and no solvent molecules were within the pores. The CPL-n cluster models were constructed based on the pore symmetry, as shown in Fig. 2, and the coordination environment of the transition metal atom, as shown in Fig. SM1 in the Supplementary Material. The cluster models for CPL-2, CPL-4, and CPL-5 are composed of one copper atom, three *pzdc*'s, and one pillar ligand for each CPL-n. The copper atom has a penta-coordination in a distorted square-pyramidal environment. These five coordinations correspond to three carboxylate oxygen atoms from the *pzdcs*, and two nitrogen atoms from the corresponding pillar-ligand and a *pzdc*. The CPL-7 cluster model is composed of two copper atoms, four *pzdc*'s, and one *bpyg*. The distance between the two copper atoms is 3.50 Å. The copper atom labeled Cu1 has a penta-coordination in a distorted trigonal-bipyramidal environment while the copper atom labeled Cu2 has a three-coordination in a distorted trigonal–pyramidal environment. For Cu1, the five coordinations correspond to the interactions with three carboxylate oxygen atoms from the *pzdc*'s and with two nitrogen atoms from a *bpyg* and a *pzdc*. The cluster models used in this work consist of 68, 70, 72, and 87 atoms for the CPL-2, CPL-4, CPL-5, and CPL-7, respectively.

For all the CPL-n models, hydrogen atoms were placed on the terminal atoms where bonds were truncated. These hydrogen atoms (link atoms) were aligned along the truncated bonds, and their positions were calculated as described by the vector $\overrightarrow{\mathbf{r}_2}$

$$\overrightarrow{\mathbf{r}_2} = \overrightarrow{\mathbf{r}_1} + g\left(\overrightarrow{\mathbf{r}_3} - \overrightarrow{\mathbf{r}_1}\right) \quad (1)$$

$$g = \frac{r_{cov(1)} + r_{cov(2)}}{r_{cov(1)} + r_{cov(3)}} \quad (2)$$

In these equations, $\overrightarrow{\mathbf{r}_1}$ and $r_{cov(1)}$ are the position vector and covalent radii, respectively, for the atoms in the pore structure that are included in the cluster model; $\overrightarrow{\mathbf{r}_3}$ and $r_{cov(3)}$ are the position vector and covalent radii, respectively, for the atoms in the pore structure that are not included in the cluster model; $\overrightarrow{\mathbf{r}_2}$ and $r_{cov(2)}$ are the position vector and the covalent radii, respectively, for the link atoms, which are not part of the pore structure, but are added into the cluster model; and g is a scale factor based

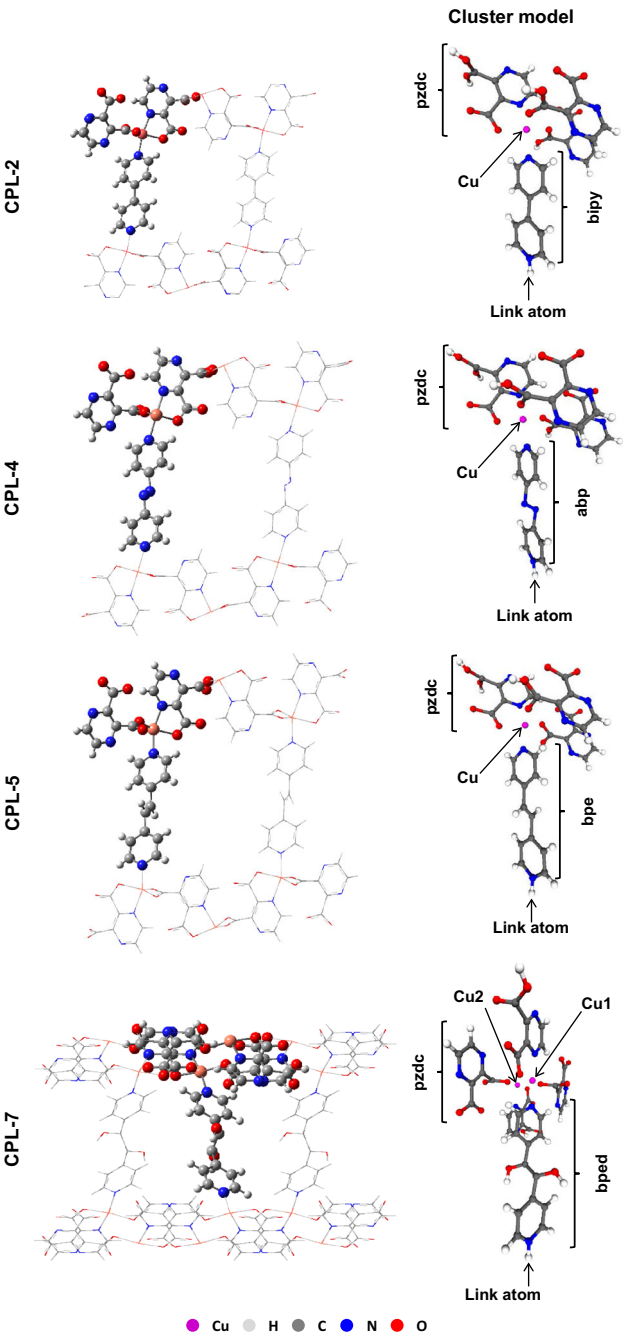

Fig. 2 Cluster models for CPL-n used in the DFT calculations: CPL-2, CPL-4, CPL-5, and CPL-7. *Magenta* copper, *blue* nitrogen, *red* oxygen, *gray* carbon, *white* hydrogen (Color figure online)

on the covalent radii (Bakowies and Thiel 1996; Byun and Morokuma 1999; Vreven et al. 2003).

2.2 Computational methods

All DFT calculations were performed using Gaussian09 (Frisch et al. 2009). We have compared two exchange/correlation functionals B3LYP (Becke 1993; Raghavachari 2001) and ωB97XD (Chai and Head-Gordon 2008). The last one is a long-range corrected hybrid density functional, which includes empirical dispersion correction, improving the description of non-covalent interactions. As opposed to ωB97XD, B3LYP has extensively been used to describe metal–organic frameworks (Baei 2013; Devic et al. 2012; Ji et al. 2014; Li et al. 2011; Liu et al. 2012). In this work, a mix of 6-311G+ (Krishnan et al. 1980; McLean and Chandler 1980) and LANL2DZ (Dunning and Hay 1976; Hay and Wadt 1985) were used for the basis sets. The latter basis set was used solely for the copper atom. It has been previously reported that the effective core potential LANL2DZ basis set can effectively describe metal atoms in metal–organic frameworks that are saturated or not exposed in the pore, such as the system that we analyzed in this study (Baei 2013; Deshmukh et al. 2013; Forrest et al. 2013; Grosch and Paesani 2012; Kim et al. 2013; Li et al. 2011; Mu et al. 2011; Wang et al. 2015a; Wang et al. 2013; Wang et al. 2015b; Zhou et al. 2011). Calculations with higher levels of theory, such as ωB97XD/aug-cc-pVDZ/D95V*+, B3LYP/aug-cc-pVDZ/D95V*+, and B2PLYPD/aug-cc-pVDZ/D95V*+, were also carried on the CPL-2 cluster to assess the performance of the methods employed in this work.

In order to determine the ground state electronic configuration of each CPL-n cluster model, single point energy calculations were performed at four different multiplicities. For the CPL-7 model, a geometry optimization was performed to calculate the relative position of the hydrogen atoms in the hydroxyl groups at *bpyg* pillar ligand. The natural bond orbital (NBO) analysis was used to quantify the electron population and partial atomic charges (Reed et al. 1985; Reed 1983; Reed and Weinhold 1985). Charges from the electrostatic potential using a grid based method (CHelpG) were also calculated (Breneman and Wiberg 1990). Electric field gradient (EFG) calculations were used to obtain electrostatic properties, such as electrostatic potential, electric field, and electric field gradient (Bjornsson and Michael 2010; Johnson et al. 1993). This type of calculation has been validated by Bjornsson and Bühl for first-row transition metal complexes (Bjornsson and Michael 2010). In their work, they compared the electric field gradient results obtained using a variety of exchange–correlation functionals and basis sets with gas phase experimental data, and they found that this method accurately captures the electrostatic properties of transition metal complexes.

In the analysis of CO_2–CPL-n interaction, different initial configurations of CO_2 relative to the CPL-n models were proposed in order to map the possible interacting sites. In all the energy minimization calculations, the CPL-n model atoms were held fixed in their crystallographic positions while the CO_2 atoms were fully optimized. The interaction energy (IE) was calculated by:

$$\mathrm{IE} = \mathrm{E}_{\mathrm{CO_2-CPL-n}} - (\mathrm{E}_{\mathrm{CO_2}} + \mathrm{E}_{\mathrm{CPL-n}}) \quad (3)$$

where $\mathrm{E}_{\mathrm{CO_2-CPL-n}}$ is the electronic energy (EE) of the optimized CO_2 molecule with the cluster model, $\mathrm{E}_{\mathrm{CO_2}}$ is the EE of the isolated CO_2 molecule, and $\mathrm{E}_{\mathrm{CPL\text{-}n}}$ is the EE of the isolated CPL-n model. All the IEs reported in this work were corrected by taking into account the basis set superposition error (BSSE) using the counterpoise method (Boys and Bernardi 1970; Simon et al. 1996). The interaction energies including the zero point energy correction are presented in the Supplementary Material.

3 Results and discussion

The adsorption interaction between an adsorbed molecule and the adsorbent framework is commonly defined by an adsorption interaction potential, Eq. 4, which describes the interaction in terms of electric permanent multipole moments for the adsorbate, and in terms electrostatic properties of the adsorbent.

$$\phi_{\mathrm{adsorbate-adsorbent}} = \phi_{\mathrm{D}} + \phi_{\mathrm{R}} + \phi_{\mathrm{ind}} + \phi_{\mathrm{F}\mu} + \phi_{\dot{\mathrm{F}}\mathrm{Q}} + \phi_{\mathrm{F}\theta} \quad (4)$$

Here, ϕ_{D} and ϕ_{R} correspond to dispersion and close-range repulsion interaction potentials, respectively, ϕ_{ind} is the induction or polarization energy, and this term arises when an heteropolar adsorbent polarizes or induces a dipole in the adsorbate, $\phi_{\mathrm{F}\mu}$, $\phi_{\dot{\mathrm{F}}\mathrm{Q}}$, and $\phi_{\mathrm{F}\theta}$ correspond to the interaction of the electric field, electric field gradient, and electric field square gradient with permanent dipole, permanent quadrupole, and permanent octapole moments, respectively (Barter 1966; Yang 2003). The following sections discuss the electrostatic properties for the CO_2 molecule, CPLs cluster models, and the CO_2–CPL-n cluster models. Partial atomic charges, electrostatic potential, and permanent multipole moments are discussed for the CO_2 molecule. A similar analysis is followed for the CPL-n that also includes the electrostatic potential and its derivatives, the electric field, and electric field gradient. Finally, an analysis of the interaction between CO_2 and the CPL-n clusters is presented.

3.1 CO_2

The geometrical features of the CO_2 molecule as well as the electron density, NBO charges, and the electrostatic potentials, as obtained with the two levels of theory used are illustrated in Fig. 3. The CO_2 is a heteronuclear molecule, with electronegativity differences between their atoms. This results in a non-uniform distributed electron density. The electron density is mainly located at the oxygen atoms, and it is equally distributed among them. The electron density distribution is also manifested in a molecular charge separation. The calculated partial atomic charges based on CHelpG and NBO schemes are listed in Tables SM1 and SM2 in the Supplementary Material. The charge distribution causes a net molecular electrostatic potential (MEP). The MEP can be mapped to illustrate the electropositive or electronegative regions in the molecule, which allowed for the identification of regions where electrostatic interactions may occur. For the CO_2 molecule, electropositive and electronegative regions are clearly noted around different parts of the molecule. The oxygen atoms are electronegative, while the electropositive region is around the carbon atom.

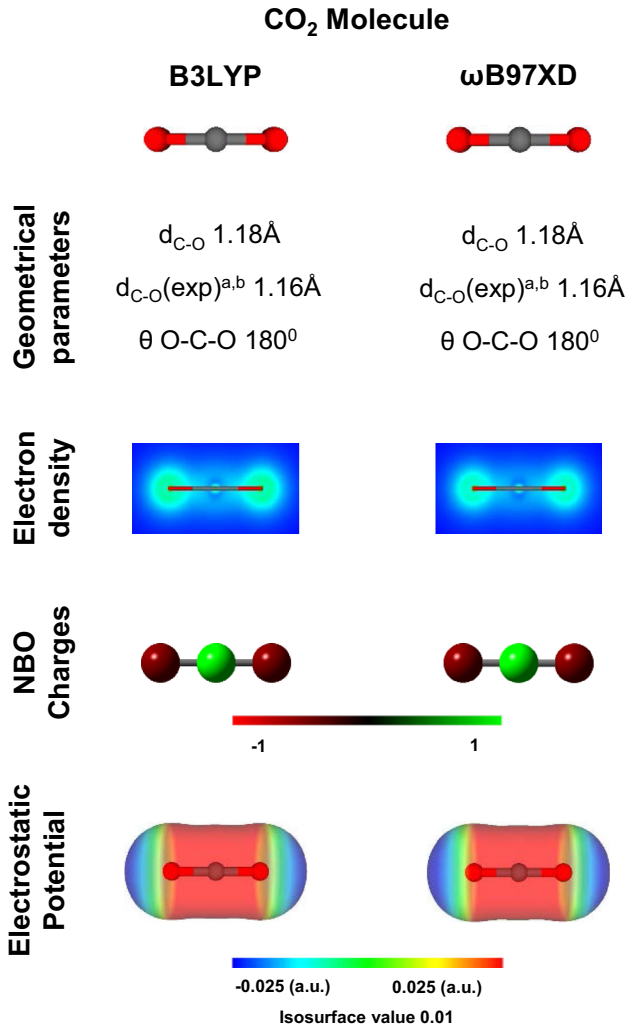

Fig. 3 CO_2 electron density, NBO atomic charges, and molecular electrostatic potential obtained with the 6-311G+ basis set. [a]Glockler (1958) and [b]Pilar (1960)

The CO_2 quadrupole moment (Θ) and the diagonal tensor components ($Q_{yy} = Q_{zz} = Q_{\perp}$ and $Q_{xx} = Q_{||}$) are listed in Tables SM3 and SM4 in the Supplementary Material. With both functionals, all diagonal components are negative, indicating the anisotropy nature of the quadrupolarity and that the charge distribution associated with the electron density is away from the molecular center of the nuclear charges; which result in a {- + -} quadrupolarity. Similar results were obtained by Glaser and co-workers (Glaser et al. 2000, 2002).

In general, both functionals give comparable results with respect to the geometrical features, the NBO charges, and the electrostatic potentials. Moreover, no significant differences between these functionals were observed when comparing other important results, such as the diagonal tensor components, the quadrupole moments, and the valence electron configurations, which are presented in Tables SM5 and SM6 in the Supplementary Material.

3.2 CPL-n models

Figures 4 and 5 illustrate electrostatic properties for CPL-n models as obtained with B3LYP and ωB97XD, respectively. The NBO charges illustrated in these figures reveal that the highest charge separation is found in the atoms located at the *pzdc*'s of the models. In all the models, the carboxylate groups show a strong charge separation between the oxygen atoms that have negative partial atomic charges, and the carbon atoms, with positive partial atomic charges. In general, the aromatic ring at the *pzdc* groups consists of neutral atoms, except for the nitrogen atoms that have a slight negative partial charge. In the CPL-7 model, a charge separation is also observed between the oxygen and the hydrogen atoms of the hydroxyl group in the *bpyg* pillar ligand. The charge separations observed in these models lead to a mixed MEP. In all the models, negative regions in the electrostatic potentials are mainly located on the *pzdc*'s of the CPL-n. On other hand, the aromatic groups of the pillar ligands exhibit electropositive potentials. However, in CPL-4 and CPL-7 small negative regions in the electrostatic potential are found on the pillar-ligands, e.g. on the nitrogen atoms of the CPL-4 pillar and on the hydroxyl group of the CPL-7 pillar. Hence, among the pillars that were analyzed in this study, only the functional groups azo (diimide) and hydroxyl in the CPL-4 and CPL-7, respectively, provide electronegative regions to the pillars of the CPL. The partial atomic charges and the

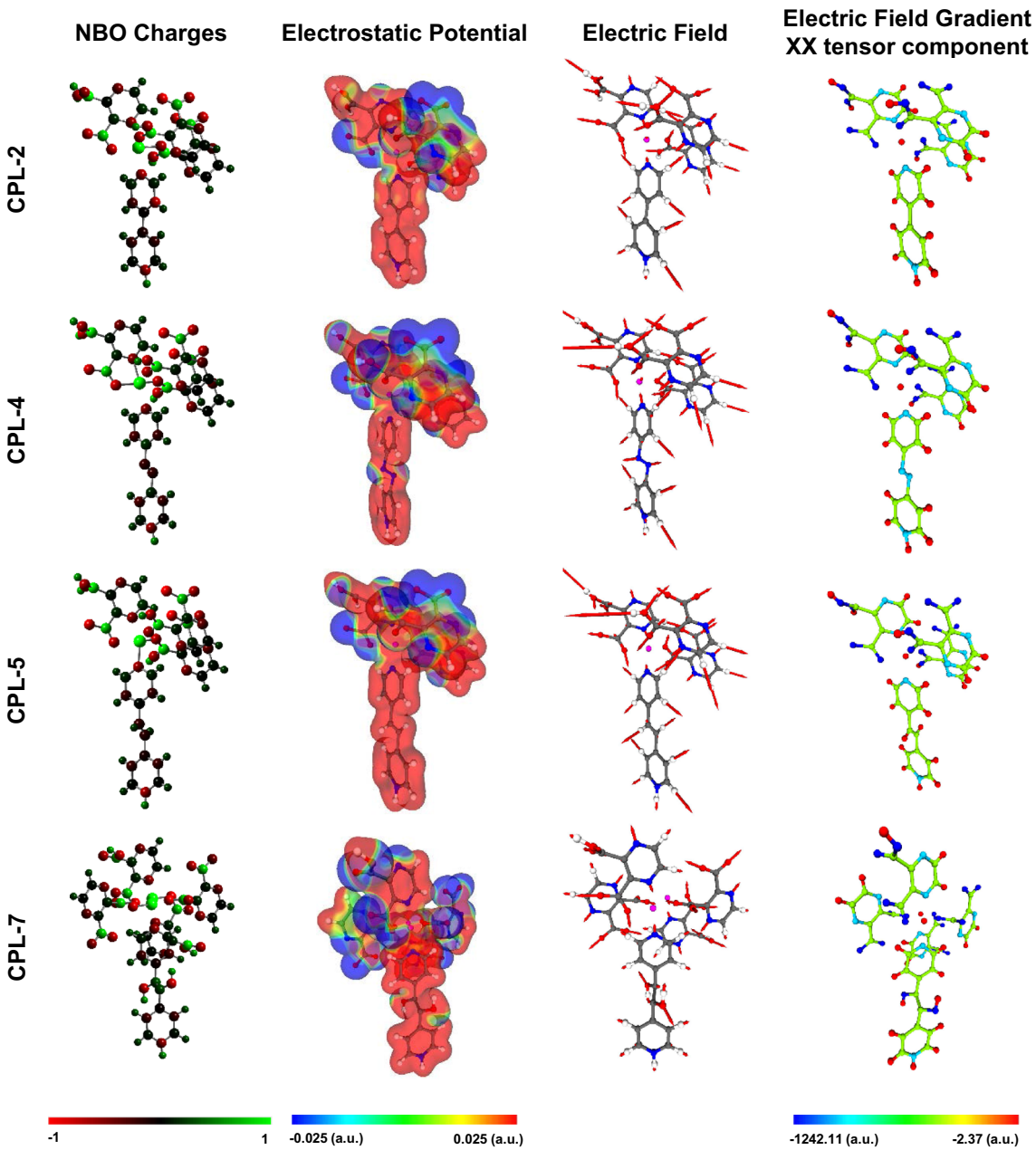

Fig. 4 NBO atomic charges, electrostatic potential, electric field and electric field gradient of the CPL-2, CPL-4, CPL-5 and CPL-7 models obtained with B3LYP

valence electronic configurations for the Cu atom within the different CPL-n analyzed in this study are tabulated in Tables SM7 and SM8 in the Supplementary Material.

Figures 4 and 5 also show the electric field and electric field gradient for each CPL-n model. As illustrated in these figures, the electric field vectors between the oxygen atoms in the carboxylate groups of the *pzdc* point in opposite directions to each other. It can also be noted that the electric field vectors on some of the hydrogen atoms of the pillar-ligands have high magnitudes compared to other vectors. However, the highest magnitudes of the electric field gradient (XX tensor component) are located on the oxygen atoms of the carboxylate groups, indicating that the highest difference in the electric field gradients is between the carbon and the oxygen atoms of that group.

In order to verify the consistency of the results obtained for electrostatic properties, NBO charges and electrostatic potential were calculated using higher levels of theory for the CPL-2 model. Figures SM3 and SM4 in the Supporting Material summarize the results. In general, no significant

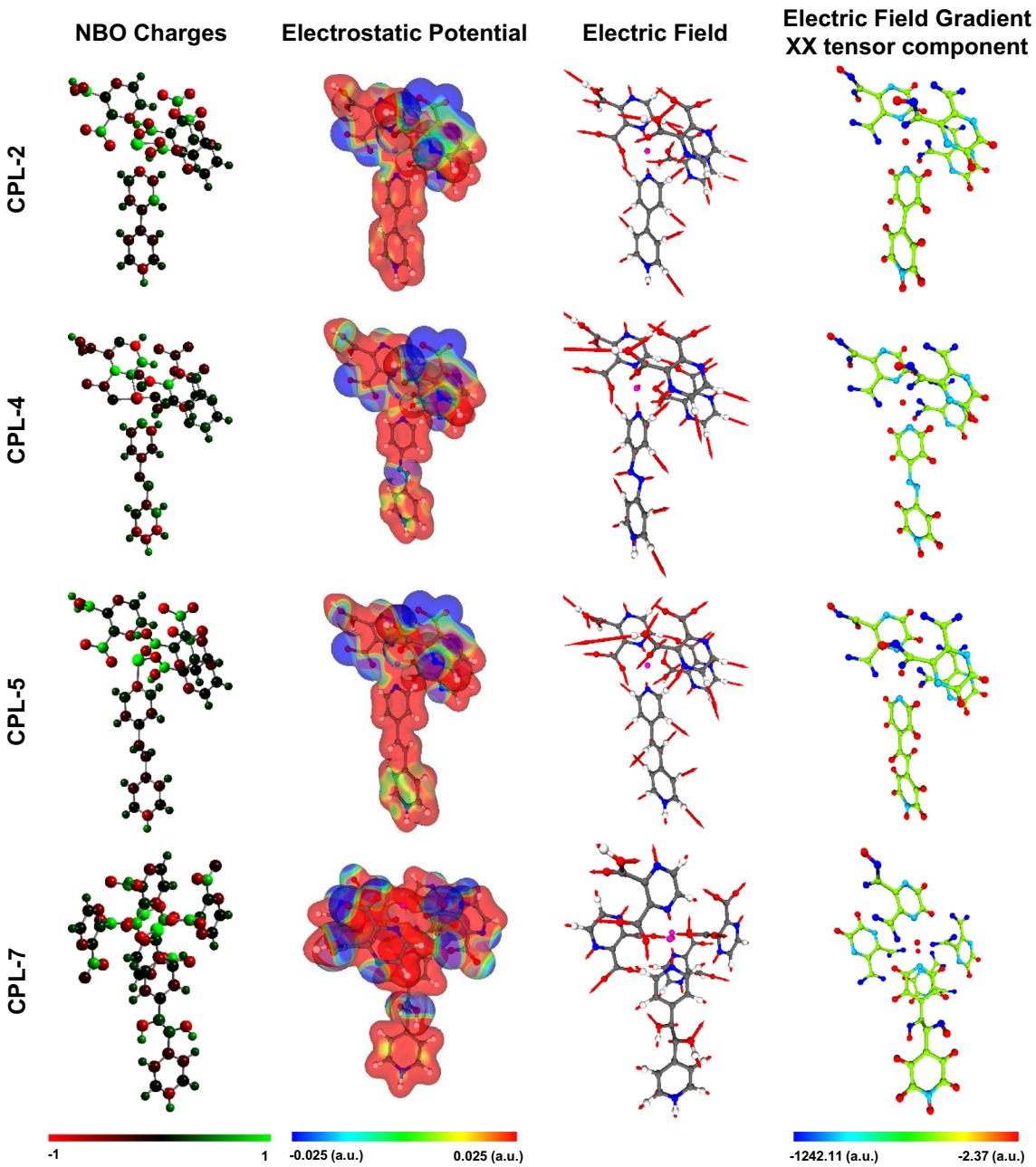

Fig. 5 NBO atomic charges, electrostatic potential, electric field and electric field gradient of the *CPL-2*, *CPL-4*, *CPL-5* and *CPL-7* models obtained with ωB97XD

differences were obtained on the NBO charges and the electrostatic potentials with the higher levels of theory. Based on these results, the NBO charge of the Cu atom has an average value of 1.02, the carboxylate groups have the strongest charge separation, and the aromatic ring at the pillar ligand has an electropositive potential. These results demonstrate that the electrostatic properties obtained with B3LYP and ωB97XD along with LANL2DZ and 6-311G+ provide an adequate description of the CPL-n's electrostatic properties.

3.3 Adsorption interaction

The range of the interaction energies (IEs) obtained for CO_2 with CPL-2, CPL-4, CPL-5 and CPL-7 models are illustrated in Fig. 6. The BSSE corrections included in the IEs had an average value of 7.20 kJ/mol for the CPL-2 systems analyzed with B3LYP. In the systems analyzed with ωB97XD, the BSSE had average values of 10.82, 10.22, 9.26, and 15.43 kJ/mol for the CPL-2, CPL-4, CPL-5 and CPL-7, respectively. As shown in Fig. 6, stronger

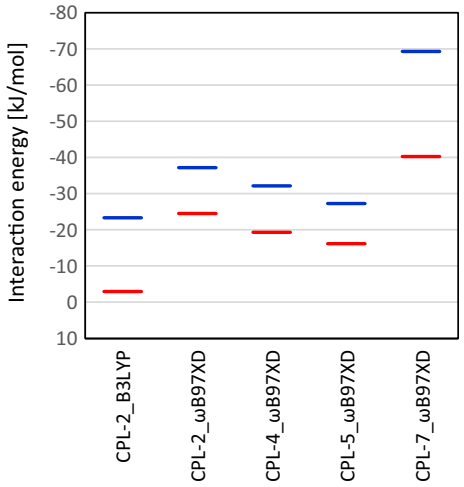

Fig. 6 Interaction energies for CO_2 with CPL-2, CPL-4, CPL-5, and CPL-7 obtained with B3LYP and ωB97XD. The lines correspond to the weakest (*red*) and strongest (*blue*) interaction for the corresponding CPL-n model (Color figure online)

interactions (lower IEs) were obtained with ωB97XD when compared to B3LYP. This difference should be expected as the ωB97XD functional includes empirical dispersion to describe long-range interactions, whereas these interactions are not accurately described in B3LYP. It is interesting to notice that, on the basis of ωB97XD, significant differences on the IEs were obtained for the CPL-7 model when compared to the other CPL-n systems. To assess the methods employed in this work, further calculations were carried out with B2PLYPD along with the basis sets aug-cc-pVDZ (Cu) and D95V+* (N, C, O and H). Single point energy calculations were performed on the configurations that yielded the strongest and weakest interactions on the CPL-2 model on the basis of ωB97XD, with IEs of −37.14 and −24.15 kJ/mol, respectively. On the basis of B2PLYPD, these configurations have IEs of −36.72 and −25.73 kJ/mol, respectively.

Figure 7 compares the optimized results of CO_2 interacting with CPL-2 obtained with B3LYP and ωB97XD. The CPL-2 model is colored gray while CO_2 is colored according to its IE. These figures allow identifying the regions where CO_2 interacts. In general, with both functionals, two interacting zones can be identified. One of them is in front of the carboxylate groups, and the second one is close to the aromatic rings of the *pzdc* group. On the basis of the results obtained with B3LYP, the strongest IEs are located near the carboxylate groups, while for ωB97XD the strongest IE is located underneath the aromatic rings of the *pzdc* layer. Hence, for the B3LYP functional, the strongest interacting site coincides with the region having the highest electric field gradient, indicating that there is a strong electrostatic contribution stabilizing these configurations. On the other hand, results obtained with the ωB97XD functional suggest that there is a strong non-electrostatic contribution that can stabilize the interaction, where there is not a significant electric field gradient.

Figure 8 illustrates the results obtained for the geometry optimizations of CO_2 with CPL-4, CPL-5, and CPL-7 as obtained with the ωB97XD functional. These results suggest that there are three interaction zones for CO_2 on these models: (1) the weakest interactions are with the pillar ligand of the model (CO_2 is colored in red in all cases), (2) near the carboxylate groups of the *pzdc* groups, and (3) below the aromatic rings of the *pzdc* groups. These zones are depicted in Fig. 9, and in each of these zones CO_2 exhibits localized interactions. For instance, in zone 1 in CPL-7 and CPL-5, one of the oxygen atoms of CO_2 interacts with a hydrogen atom of the pillar. In this zone, IEs are between −69.29 and −16.20 kJ/mol. In the configurations depicted in zone 2, the carbon atom of CO_2

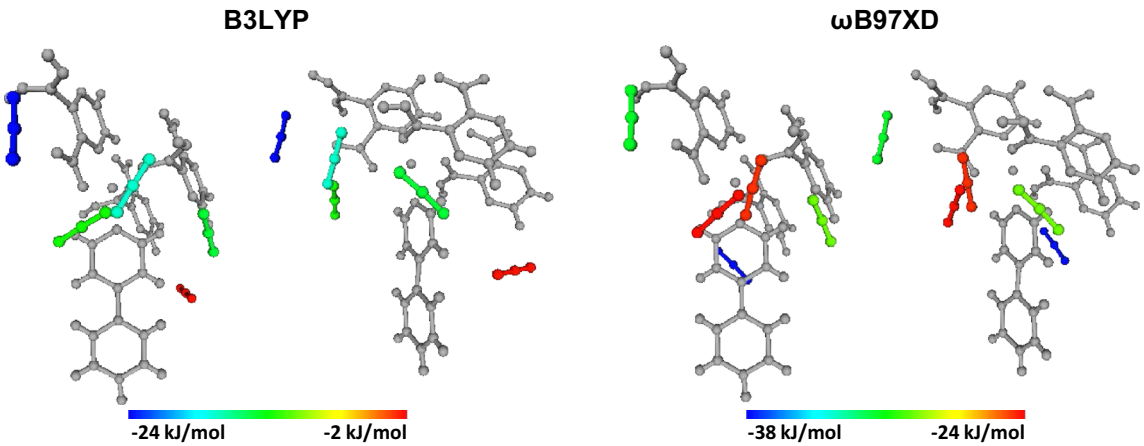

Fig. 7 Minimum energy configurations of CO_2 interacting with CPL-2 as obtained with B3LYP (*left*) and ωB97XD (*right*). Atoms corresponding to the CPL-2 framework are *colored gray*, and the CO_2 molecules are colored according to the IE as indicated in the *color legends* (Color figure online)

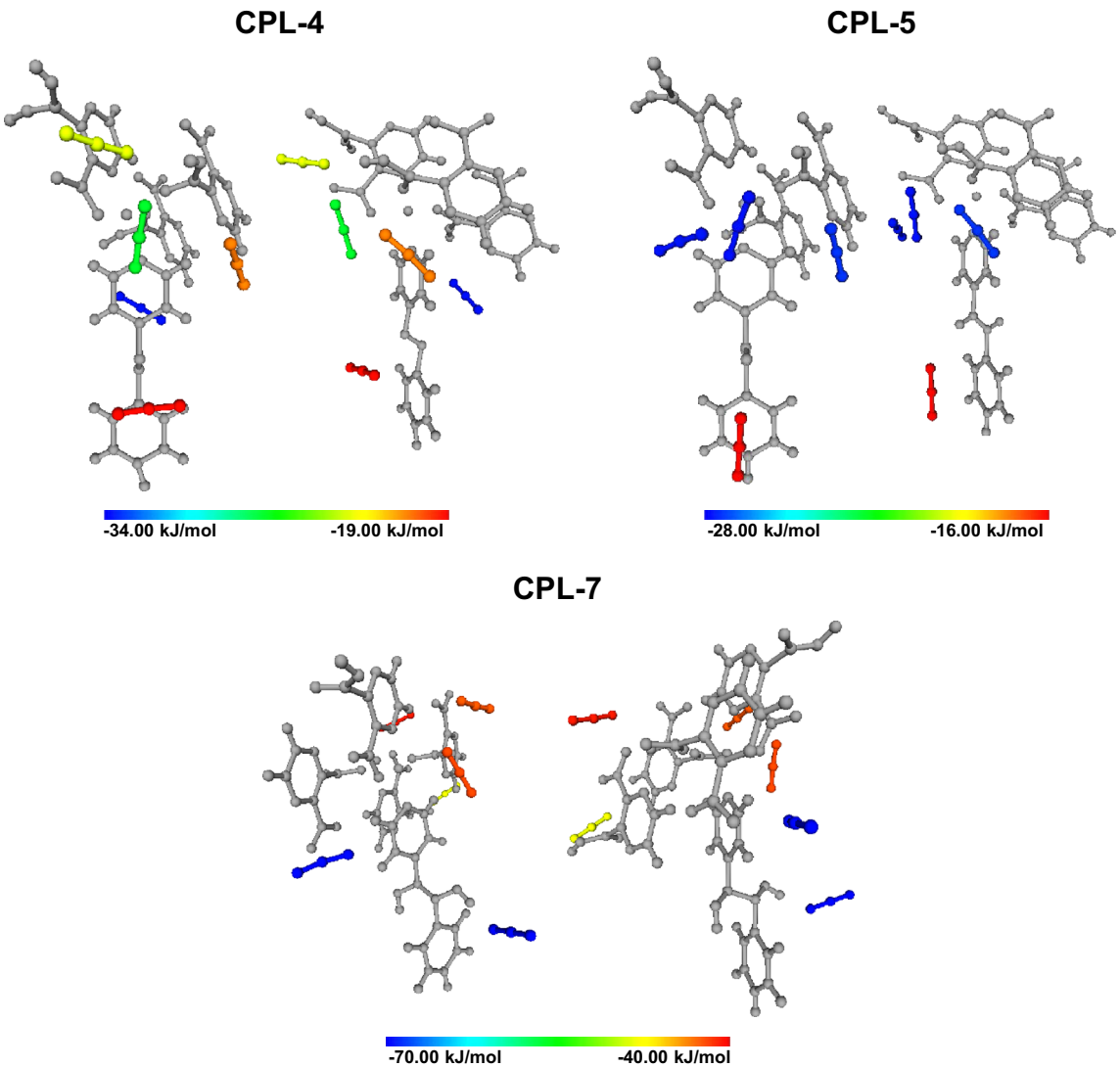

Fig. 8 Optimized geometries of CO_2 interacting with CPL-4 (*top left*), CPL-5 (*top right*), and CPL-7 (*bottom*) as obtained with ωB97XD. Atoms corresponding to the CPL-4, CPL-5, and CPL-7 frameworks are *colored gray*, and the CO_2 molecules are colored according to the IE as indicated in the *color legends* (Color figure online)

interacts with the oxygen atom of the carboxylate groups. With CPL-2, CPL-4 and CPL-5 the IEs are on average −28.5 kJ/mol, and in the CPL-7 the IE is −69.06 kJ/mol. In zone 3, the carbon atom of the CO_2 is approximately 3 Å from the nitrogen atom of one of the *pzdc* rings. This interaction was only observed on CPL-2, CPL-4, and CPL-5, and the IE has an average value of −32.14 kJ/mol. Figures SM5 to SM9 in the Supplementary Material illustrate each of the CO_2 interaction configurations obtained for all the CPL-n models analyzed in this study. For instance, on CPL-4 the strongest interaction with CO_2 (IE = −33.12 kJ/mol) was obtained when the carbon atom and one oxygen atom of CO_2 interact with the nitrogen atom and one hydrogen atom on the aromatic ring in the *pzdc* group. For CPL-5 and CPL-7, the strongest interactions with IEs of −27.28 and −69.29 kJ/mol, respectively are located close to the carboxylate groups of the layer.

Interestingly, in one of the minimum energy configurations obtained for CO_2 with CPL-7, the carbon atom of CO_2 binds to one of the oxygen atoms of the carboxylate group of the layer. The distance between these atoms is 1.67 Å. In this configuration, illustrated in Fig. SM9-(a) in the Supplementary Material, CO_2 loses its linearity, forming an O–C–O angle of 140.3°. Based on the NBO results, in Table SM9 in the Supplementary Material, this bend occurs upon chemical bond formation between the carbon and the oxygen atom. This result is consistent with several theoretical and experimental works that have reported similar CO_2 interactions in other systems in which

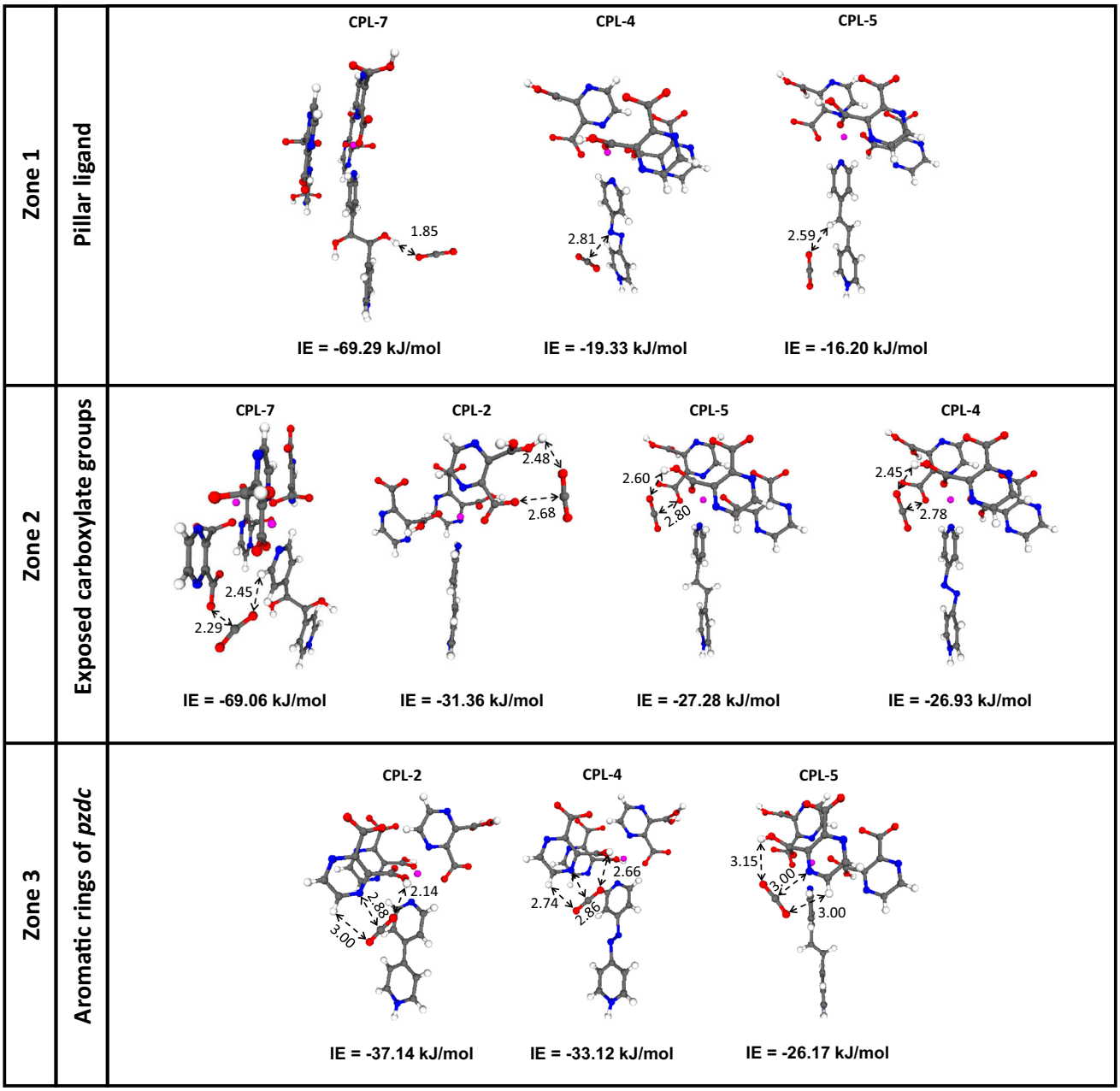

Fig. 9 CO_2 interaction zones for CPL-2, CPL-4, CPL-5, and CPL-7 models obtained with ωB97XD

Table 1 Change in electron occupancy of CO_2 upon interaction with the CPL-n systems on the lowest IE configuration

Atom	CO_2–CPL-2 B3LYP	CO_2–CPL-2 ωB97XD	CO_2–CPL-4	CO_2–CPL-5	CO_2–CPL-7
O	0.07911	0.07124	0.05718	0.02230	0.02621
C	−0.04377	−0.04329	−0.03679	−0.03355	−0.06464
O	−0.03111	−0.02719	−0.01604	0.01101	0.10564
Total	4.23×10^{-3}	7.6×10^{-4}	4.35×10^{-3}	-2.4×10^{-4}	6.721×10^{-2}

CO_2 is chemisorbed (Davran-Candan 2014; Ismael et al. 2009; Oktavian et al. 2014; da Silva and Svendsen 2007; Yamada et al. 2014; Yamada et al. 2011).

Since it is expected that one of the main contributions to the interaction of CO_2 and CPL-n materials is the electrostatic interaction, the electrostatic potential for each CO_2

optimized configuration was also analyzed. The electrostatic potential for all the configurations obtained in this study are presented in Figs. SM5 to SM9 in the Supplementary Material. As illustrated in these figures, the negative region in the MEP of CO_2 changes significantly when compared to the isolated CO_2 molecule. In general, for each of the CO_2 interaction configurations, it can be noted a change of the electrostatic potential of the interacting CO_2 compared to the electrostatic potential of the isolated CO_2, particularly around the oxygen atoms. For example, in the configurations that yield the strongest interactions in CPL-2 and in CPL-4, the electrostatic potential become electropositive on one of the oxygen atoms. And in the configuration with the strongest interaction on the CPL-7 model, the MEP becomes electropositive. In the CPL-5 model, however, it can be noted that the electrostatic potential for the CO_2 remains {- + -}. Nevertheless, the electronegative potential of CO_2 interacts through the electropositive regions of the CPL-n cluster model, and the electropositive potential of the CO_2 interacts with an electronegative region of the CPL-n. These results suggest that in most cases, the interaction is dictated by the coupling of the electrostatic potential between the CO_2 and the CPL-n model. Hence, the CPLs structures encourage a cooperative intermolecular interaction with the CO_2 by virtue of a pore-wall mixed electrostatic potential environment and the electrostatic nature of the CO_2 molecule.

The observed changes in the electrostatic potential of CO_2 upon the interaction can be related to a change of the CO_2 electron population. Table 1 lists the change of electron occupancy of CO_2 upon interaction with the CPL-n models for the lowest IE. A negative sign indicates a decline in the electron occupancy upon the interaction. In all the cases, the carbon atom and one of the oxygen atoms decrease and increase, respectively, the electron occupancy, while the other oxygen atom may increase or decrease its the electron occupancy. These results indicate that not only the electrostatic and dispersion contributions stabilize the interaction, but also there is a slight charge transfer that contributes to the interaction stabilization.

4 Conclusions

Based on the electrostatic properties of the CPLs and CO_2, we have unraveled fundamental aspects related to the nature of the CO_2–CPL-n interaction. Our results demonstrate that the electrostatic properties (atomic charges, electrostatic potentials, electric field and electric field gradient) of the CPLs analyzed in this study allow to identify chemical functionalities that promote the interaction with CO_2. Moreover, we mapped different CO_2 interaction zones and related them to the electrostatic properties of the CPL-n materials. Our calculations demonstrate that the carboxylate groups at *pzdc* layer have a large electron density separation, which results in a high electric field gradient, promoting electrostatic interactions. Additionally, the presence of chemical functionalities in the pillar of CPLs also favors the interaction with CO_2. The electrostatic potentials show how the potential of the CO_2 molecule change upon interaction with the different CPL-n. Thus, not only the electrostatic and dispersion contributions stabilize the interaction, but also slight charge transfer takes place upon the interaction.

In general, most of the IEs obtained are in the range of physical adsorption, and the geometry of the CO_2 molecule upon interaction was, in most cases, comparable to the isolated molecule. However, for the CPL-7 system, the strongest interaction site resulted in an O–C–O angle of 140°, and a chemical bond was formed between the carbon from the CO_2 molecule and an oxygen atom of a carboxylate group.

Acknowledgments This research was supported by NSF-CREST (Grant Number HRD-0833112) and NASA EPSCoR (Grant Number NNX13AD38A). This research used computational resources of the National Energy Research Scientific Computing Center, which is supported by the Office of Science of the U.S. Department of Energy under Contract No. DE-AC02-05CH11231, and the High-Performance Computing Facility of the Institute for Functional Nanomaterials, which is supported by NSF through Grants EPS-1002410 and EPS 1010094. The authors thank to Prof. Arturo Hernández-Maldonado and Jose Primera-Pedrozo for helpful discussions.

References

Bae, Y.-S., Snurr, R.Q.: Development and evaluation of porous materials for carbon dioxide separation and capture. Angew. Chem. Int. Ed. Engl. **50**, 11586–11596 (2011)

Bae, Y.-S., Moon, J.-H., Ahn, H., Lee, C.-H.: Effects of adsorbate properties on adsorption mechanism in a carbon molecular sieve. Korean J. Chem. Eng. **21**, 712–720 (2004)

Baei, M.: DFT study of CO_2 adsorption on the $Zn_{12}O_{12}$ nano-cage. Bull. Korean Chem. Soc. **34**, 3722–3726 (2013)

Bakowies, D., Thiel, W.: Hybrid models for combined quantum mechanical and molecular mechanical approaches. J. Phys. Chem. **3654**, 10580–10594 (1996)

Barter, R.M.: Specificity in physical sorption. J. Colloid Interface Sci. **21**, 415–434 (1966)

Becke, A.D.: Density-functional thermochemistry. III. The role of exact exchange. J. Chem. Phys. **98**, 5648–5652 (1993)

Bjornsson, R., Michael, B.: Electric field gradients of transition metal complexes from density functional theory: assessment of functionals, geometries and basis sets. Dalt. Trans. **39**, 5319–5324 (2010)

Boys, S.F., Bernardi, F.: The calculation of small molecular interactions by the differences of separate total energies. Some procedures with reduced errors. Mol. Phys. **19**, 553–566 (1970)

Breneman, C.M., Wiberg, K.B.: Determining atom-centered monopoles from molecular electrostatic potentials. The need for high sampling density in formamide conformational analysis. J. Comput. Chem. **11**, 361–373 (1990)

Byun, K.S., Morokuma, K.: A new ONIOM implementation in Gaussian98. Part I. The calculation of energies, gradients, vibrational frequencies and electric field derivatives. J. Mol. Struct. **461**, 1–21 (1999)

Chai, J.-D., Head-Gordon, M.: Long-range corrected hybrid density functionals with damped atom-atom dispersion corrections. Phys. Chem. Chem. Phys. **10**, 6615–6620 (2008)

Choi, S., Drese, J.H., Jones, C.W.: Adsorbent materials for carbon dioxide capture from large anthropogenic point sources. ChemSusChem. **2**, 796–854 (2009)

Culp, J.T., Chen, D.-L., Liu, J., Chirdon, D., Kauffman, K., Goodman, A., Johnson, J.K.: Effect of spin-crossover-induced pore contraction on CO_2-host interactions in the porous coordination polymers [Fe(pyrazine)M(CN)$_4$] (M = Ni, Pt). Eur. J. Inorg. Chem. **2013**, 511–519 (2013)

Da Silva, E.F., Svendsen, H.F.: Computational chemistry study of reactions, equilibrium and kinetics of chemical CO_2 absorption. Int. J. Greenh. Gas Control. **1**, 151–157 (2007)

Davran-Candan, T.: DFT modeling of CO_2 interaction with various aqueous amine structures. J. Phys. Chem. A **118**, 4582–4590 (2014)

Deshmukh, M.M., Ohba, M., Kitagawa, S., Sakaki, S.: Absorption of CO_2 and CS_2 into the Hofmann-type porous coordination polymer: electrostatic versus dispersion interactions. J. Am. Chem. Soc. **135**, 4840–4849 (2013)

Devic, T., Salles, F., Bourrelly, S., Moulin, B., Maurin, G., Horcajada, P., Serre, C., Vimont, A., Lavalley, J.-C., Leclerc, H., Clet, G., Daturi, M., Llewellyn, P.L., Filinchuk, Y., Férey, G.: Effect of the organic functionalization of flexible MOFs on the adsorption of CO_2. J. Mater. Chem. **22**, 10266–10273 (2012)

Dunning, T.H.J., Hay, P.J.: Gaussian basis sets for molecular calculations. In: Schaefer, H.F.I. (ed.) Modern Theoretical Chemistry, pp. 1–28. Plenum, New York (1976)

Forrest, K.A., Pham, T., Hogan, A., Mclaughlin, K., Tudor, B., Nugent, P., Burd, S.D., Mullen, A., Cioce, C.R., Wojtas, L., Zaworotko, M.J., Space, B.: Computational studies of CO_2 sorption and separation in an ultramicroporous metal–organic material. J. Phys. Chem. C **117**, 17687–17698 (2013)

Frisch, M.J., Trucks, G.W., Schlegel, H.B., Scuseria, G.E., Robb, M.A., Cheeseman, J.R., Scalmani, G., Barone, V., Mennucci, B., Petersson, G.A., Nakatsuji, H., Caricato, M., Li, X., Hratchian, H.P., Izmaylov, A.F., Bloino, J., Zheng, G., Sonnenberg, J.L., Hada, M., Ehara, M., Toyota, K., Fukuda, R., Hasegawa, J., Ishida, M., Nakajima, T., Honda, Y., Kitao, O., Nakai, H., Vreven, T., Montgomery, J.A., Peralta, J.E.J., Ogliaro, F., Bearpark, M., Heyd, J.J., Brothers, E., Kudin, K.N., Staroverov, V.N., Kobayashi, R., Normand, J., Raghavachari, K., Rendell, A., Burant, J.C., Iyengar, S.S., Tomasi, J., Cossi, M., Rega, N., Millam, J.M., Klene, M., Knox, J.E., Cross, J.B., Bakken, V., Adamo, C., Jaramillo, J., Gomperts, R., Stratmann, R.E., Yazyev, O., Austin, A.J., Cammi, R., Pomelli, C., Ochterski, J.W., Martin, R.L., Morokuma, K., Zakrzewski, V.G., Voth, G.A., Salvador, P., Dannenberg, J.J., Dapprich, S., Daniels, A.D., Farkas, O., Foresman, J.B., Ortiz, J. V., Cioslowski, J., Fox, D.J.: Guassian 09, http://www.gaussian.com/ (2009)

García-Ricard, O.J., Hernández-Maldonado, A.J.: Cu_2(pyrazine-2,3-dicarboxylate)$_2$(4,4′-bipyridine) porous coordination sorbents: activation temperature, textural properties, and CO_2 adsorption at low pressure range. J. Phys. Chem. C **114**, 1827–1834 (2010)

García-Ricard, O.J., Fu, R., Hernández-Maldonado, A.J.: Thermally induced changes in a porous coordination polymer Cu_2(pyrazine-2,3-dicarboxylate)2(4,4′-bipyridine) studied via in situ X-ray diffraction and 13C cross-polarization magic angle spinning nuclear magnetic resonance spectroscopy. J. Phys. Chem. C **115**, 3595–3601 (2011)

García-Ricard, O.J., Silva-Martínez, J.C., Hernández-Maldonado, A.J.: Systematic evaluation of textural properties, activation temperature and gas uptake of $Cu_2(pzdc)_2L$ [L = dipyridyl-based ligands] porous coordination pillared-layer networks. Dalt. Trans. **41**, 8922–8930 (2012)

García-Ricard, O.J., Meza-Morales, P., Silva-Martínez, J.C., Curet-Arana, M.C., Hogan, J.A., Hernández-Maldonado, A.J.: Carbon dioxide storage and sustained delivery by $Cu_2(pzdc)_2L$ [L = dipyridyl-based ligand] pillared-layer porous coordination networks. Microporous Mesoporous Mater. **177**, 54–58 (2013)

Glaser, R., Wu, Z., Lewis, M.: A higher level ab initio quantum-mechanical study of the quadrupole moment tensor components of carbon dioxide. J. Mol. Struct. **556**, 131–141 (2000)

Glaser, R., Lewis, M., Wu, Z.: Theoretical study of the quadrupolarity of carbodiimide. J. Phys. Chem. A **106**, 7950–7957 (2002)

Glockler, G.: Carbon-oxygen bond energies and bond distances. J. Phys. Chem. **62**, 1049–1054 (1958)

Grajciar, L., Wiersum, A.D., Llewellyn, P.L., Chang, J., Nachtigall, P.: Understanding CO_2 adsorption in CuBTC MOF: comparing combined DFT-ab initio calculations with microcalorimetry experiments. J. Phys. Chem. C **115**, 17925–17933 (2011)

Grajciar, L., Nachtigall, P., Bludský, O., Rubeš, M.: Accurate ab initio description of adsorption on coordinatively unsaturated Cu^{2+} and Fe^{3+} sites in MOFs. J. Chem. Theory Comput. **11**, 230–238 (2015)

Grosch, J.S., Paesani, F.: Molecular-level characterization of the breathing behavior of the jungle-gym-type DMOF-1 metal-organic framework. J. Am. Chem. Soc. **134**, 4207–4215 (2012)

Harries, J.E.: The quadrupole moment of CO_2, measured from the far infrared spectrum. J. Phys. B **3**, 150–152 (1970)

Haskopoulos, A., Maroulis, G.: Dipole and quadrupole (hyper)polarizability for the asymmetric stretching of carbon dioxide: improved agreement between theory and experiment. Chem. Phys. Lett. **417**, 235–240 (2006)

Hay, P.J., Wadt, W.R.: Ab initio effective core potentials for molecular calculations. Potentials for the transition metal atoms Sc to Hg. J. Chem. Phys. **82**, 270–283 (1985)

Hijikata, Y., Sakaki, S.: Interaction of various gas molecules with paddle-wheel-type open metal sites of porous coordination polymers: theoretical investigation. Inorg. Chem. **53**, 2417–2426 (2014)

Ismael, M., Sahnoun, R., Suzuki, A., Koyama, M., Tsuboi, H., Hatakeyama, N., Endou, A., Takaba, H., Kubo, M., Shimizu, S., Del Carpio, C.A., Miyamoto, A.: A DFT study on the carbamates formation through the absorption of CO_2 by AMP. Int. J. Greenh. Gas Control. **3**, 612–616 (2009)

Ji, H., Park, J., Cho, M., Jung, Y.: Assessments of semilocal density functionals and corrections for carbon dioxide adsorption on metal-organic frameworks. ChemPhysChem **15**, 3157–3165 (2014)

Johnson, B.G., Gill, P.M.W., Pople, J.A., Fox, D.J.: Computing molecular electrostatic potentials with the PRISM algorithm. Chem. Phys. Lett. **206**, 239–246 (1993)

Kim, K.C., Yu, D., Snurr, R.Q.: Computational screening of functional groups for ammonia capture in metal-organic frameworks. Langmuir **29**, 1446–1456 (2013)

Kitagawa, S., Kitaura, R., Noro, S.: Functional porous coordination polymers. Angew. Chem. Int. Ed. **43**, 2334–2375 (2004)

Kitaura, R., Fujimoto, K., Noro, S., Kondo, M., Kitagawa, S.: A pillared-layer coordination polymer network displaying hysteretic sorption: [$Cu_2(pzdc)_2$(dpyg)]n (pzdc = Pyrazine-2,3-dicarboxylate; dpyg = 1,2-di(4-pyridyl)-glycol). Angew. Chemie Int. Ed. **41**, 133–135 (2002)

Kondo, M., Okubo, T., Asami, A., Noro, S., Yoshitomi, T., Kitagawa, S., Ishii, T., Matsuzaka, H., Seki, K.: Rational synthesis of stable channel-like cavities with methane gas adsorption properties: [{$Cu_2(pzdc)(L)_n$](pzdc = pyra-zine-2,3-dicarboxylate; L = a Pillar Ligand). Angew. Chemie Int. Ed. **38**, 140–143 (1999)

Krishnan, R., Binkley, J.S., Seeger, R., Pople, J.A.: Self-consistent molecular orbital methods. XX. A basis set for correlated wave functions. J. Chem. Phys. **72**, 650–654 (1980)

Kuppler, R.J., Timmons, D.J., Fang, Q.-R., Li, J.-R., Makal, T.A., Young, M.D., Yuan, D., Zhao, D., Zhuang, W., Zhou, H.-C.: Potential applications of metal-organic frameworks. Coord. Chem. Rev. **253**, 3042–3066 (2009)

Lewis, M., Wu, Z., Glaser, R.: Polarizabilities of carbon dioxide and carbodiimide. Assessment of theoretical model dependencies on dipole polarizabilities and dipole polarizability anisotropies †. J. Phys. Chem. A **104**, 11355–11361 (2000)

Li, J.-R., Kuppler, R.J., Zhou, H.-C.: Selective gas adsorption and separation in metal–organic frameworks. Chem. Soc. Rev. **38**, 1477–1504 (2009)

Li, J.-R., Ma, Y., McCarthy, M.C., Sculley, J., Yu, J., Jeong, H.-K., Balbuena, P.B., Zhou, H.-C.: Carbon dioxide capture-related gas adsorption and separation in metal-organic frameworks. Coord. Chem. Rev. **255**, 1791–1823 (2011)

Li, J.-R., Sculley, J., Zhou, H.-C.: Metal–organic frameworks for separations. Chem. Rev. **112**, 869–932 (2012)

Liu, Y., Liu, J., Chang, M., Zheng, C.: Theoretical studies of CO_2 adsorption mechanism on linkers of metal–organic frameworks. Fuel **95**, 521–527 (2012)

Maroulis, G.: Electric (hyper)polarizability derivatives for the symmetric stretching of carbon dioxide. Chem. Phys. **291**, 81–95 (2003)

Maroulis, G.: A note on the electric multipole moments of carbon dioxide. Chem. Phys. Lett. **396**, 66–68 (2004)

Matsuda, R., Tsujino, T., Sato, H., Kubota, Y., Morishige, K., Takata, M., Kitagawa, S.: Temperature responsive channel uniformity impacts on highly guest-selective adsorption in a porous coordination polymer. Chem. Sci. **1**, 315–321 (2010)

McLean, A.D., Chandler, G.S.: Contracted Gaussian basis sets for molecular calculations. I. Second row atoms, $Z = 11$–18. J. Chem. Phys. **72**, 5639–5648 (1980)

Millward, A.R., Yaghi, O.M.: Metal–organic frameworks with exceptionally high capacity for storage of carbon dioxide at room temperature. J. Am. Chem. Soc. **127**, 17998–17999 (2005)

Mu, W., Liu, D., Zhong, C.: A computational study of the effect of doping metals on CO_2/CH_4 separation in metal–organic frameworks. Microporous Mesoporous Mater. **143**, 66–72 (2011)

Nijem, N., Thissen, P., Yao, Y., Longo, R.C., Roodenko, K., Wu, H., Zhao, Y., Cho, K., Li, J., Langreth, D.C., Chabal, Y.J.: Understanding the preferential adsorption of CO_2 over N_2 in a flexible metal–organic framework. J. Am. Chem. Soc. **133**, 12849–12857 (2011)

Noro, S., Kitagawa, S., Kondo, M., Seki, K.: A new, methane adsorbent, porous coordination polymer $[\{CuSiF_6(4,4'\text{-bypyridine})_2\}_n]$. Angew. Chemie Int. Ed. **39**, 2081–2084 (2000)

Noro, S., Hijikata, Y., Inukai, M., Fukushima, T., Horike, S., Higuchi, M., Kitagawa, S., Akutagawa, T., Nakamura, T.: Highly selective CO_2 adsorption accompanied with low-energy regeneration in a two-dimensional Cu(II) porous coordination polymer with inorganic fluorinated PF_6^- anions. Inorg. Chem. **52**, 280–285 (2013)

Oktavian, R., Taha, M., Lee, M.: Experimental and computational study of co_2 storage and sequestration with aqueous 2-amino-2-hydroxymethyl-1,3-propanediol (TRIS) solutions. J. Phys. Chem. A **118**, 11572–11582 (2014)

Pianwanit, A., Kritayakornupong, C., Vongachariya, A., Selphusit, N., Ploymeerusmee, T., Remsungnen, T., Nuntasri, D., Fritzsche, S., Hannongbua, S.: The optimal binding sites of CH_4 and CO_2 molecules on the metal-organic framework MOF-5: ONIOM calculations. Chem. Phys. **349**, 77–82 (2008)

Pilar, F.L.: Bond-order/bond-length and bond-energy/bond-length relations for carbon-oxygen bonds. J. Mol. Spectrosc. **5**, 72–77 (1960)

Raghavachari, K.: Perspective on "DENSITY functional thermochemistry. III. The role of exact exchange". In: Cramer, C.J., Truhlar, D.G. (eds.) Theoretical Chemistry Accounts, pp. 361–363. Springer, Berlin (2001)

Ramsahye, N.A., Maurin, G., Bourrelly, S., Llewellyn, P.L., Serre, C., Loiseau, T., Devic, T., Ferey, G.: Probing the adsorption sites for CO_2 in metal organic frameworks materials MIL-53 (Al, Cr) and MIL-47 (V) by density functional theory. J. Phys. Chem. **112**, 514–520 (2008)

Reed, A.E.: Natural bond orbital analysis of near-Hartree–Fock water dimer. J. Chem. Phys. **78**, 4066–4073 (1983)

Reed, A.E., Weinhold, F.: Natural localized molecular orbitals. J. Chem. Phys. **83**, 1736–1740 (1985)

Reed, A.E., Weinstock, R.B., Weinhold, F.: Natural population analysis. J. Chem. Phys. **83**, 735–746 (1985)

Rezakazemi, M., Ebadi Amooghin, A., Montazer-Rahmati, M.M., Ismail, A.F., Matsuura, T.: State-of-the-art membrane based CO_2 separation using mixed matrix membranes (MMMs): an overview on current status and future directions. Prog. Polym. Sci. **39**, 817–861 (2014)

Sakamoto, H., Kitaura, R., Matsuda, R., Kitagawa, S., Kubota, Y., Takata, M.: Systematic construction of porous coordination pillared-layer structures and their sorption properties. Chem. Lett. **39**, 218–219 (2010)

Simon, S., Duran, M., Dannenberg, J.J.: How does basis set superposition error change the potential surfaces for hydrogen-bonded dimers? J. Chem. Phys. **105**, 11024 (1996)

Songolzadeh, M., Ravanchi, M.T., Soleimani, M.: Carbon dioxide capture and storage: a general review on adsorbents. World Acad. Sci. Eng. Technol. **70**, 225–232 (2012)

Sumida, K., Rogow, D.L., Mason, J.A., McDonald, T.M., Bloch, E.D., Herm, Z.R., Bae, T.-H., Long, J.R.: Carbon dioxide capture in metal-organic frameworks. Chem. Rev. **112**, 724–781 (2012)

Uemura, T., Kitaura, R., Ohta, Y., Nagaoka, M., Kitagawa, S.: Nanochannel-promoted polymerization of substituted acetylenes in porous coordination polymers. Angew. Chem. Int. Ed. Engl. **45**, 4112–4116 (2006)

Uribe-romo, F.J., Knobler, C.B., Keeffe, M.O., Yaghi, O.M.: Synthesis, structure, and carbon dioxide capture properties of zeolitic imidazolate frameworks. Acc. Chem. Res. **43**, 58–67 (2010)

Vaidhyanathan, R., Iremonger, S.S., Shimizu, G.K.H., Boyd, P.G., Alavi, S., Woo, T.K.: Direct observation and quantification of CO_2 binding within an amine-functionalized nanoporous solid. Science **330**, 650–653 (2010)

Varanasi, P.: On the quadrupole moment of CO_2. J. Chem. Phys. **53**, 4404–4405 (1970)

Vreven, T., Morokuma, K., Farkas, O., Schlegel, H.B., Frisch, M.J.: Geometry optimization with QM/MM, ONIOM, and other combined methods. I. Microiterations and constraints. J. Comput. Chem. **24**, 760–769 (2003)

Wang, S., Yang, Q., Zhang, J., Zhang, X., Zhao, C., Jiang, L., Su, C.Y.: Two-dimensional charge-separated metal-organic framework for hysteretic and modulated sorption. Inorg. Chem. **52**, 4198–4204 (2013)

Wang, N., Liu, Y., Qiao, Z., Diestel, L., Zhou, J., Huang, A., Caro, J.: Polydopamine-based synthesis of a zeolite imidazolate framework ZIF-100 membrane with high H_2/CO_2 selectivity. J. Mater. Chem. A. **3**, 4722–4728 (2015a)

Wang, W., Zhang, X., Li, P., Sun, Q., Li, Z., Ren, C., Guo, C.: CO_2 capture and separation from N_2/CH_4 mixtures by $Co@B_8/Co@B_8^-$ and $M@B_9/M@B_9^-$ ($M = Ir, Rh, Ru$) clusters: a theoretical study. J. Phys. Chem. A **119**, 796–805 (2015b)

Yamada, H., Matsuzaki, Y., Higashii, T., Kazama, S.: Density functional theory study on carbon dioxide absorption into aqueous solutions of 2-amino-2-methyl-1-propanol using a

continuum solvation model. J. Phys. Chem. A **115**, 3079–3086 (2011)
Yamada, H., Matsuzaki, Y., Goto, K.: Quantitative spectroscopic study of equilibrium in CO_2-loaded aqueous 2-(ethylamino) ethanol solutions. Ind. Eng. Chem. Res. **53**, 1617–1623 (2014)
Yang, R.T.: ADSORBENTS Fundamentals and Applications. Wiley, New Jersey (2003)
Yu, C.-H.: A review of CO_2 capture by absorption and adsorption. Aerosol Air Qual. Res. **12**, 745–769 (2012)
Yu, J., Balbuena, P.B.: Water effects on postcombustion CO_2 capture in Mg-MOF-74. J. Phys. Chem. C **117**, 3383–3388 (2013)
Zhou, C., Cao, L., Wei, S., Zhang, Q., Chen, L.: A first principles study of gas adsorption on charged Cu-BTC. Comput. Theor. Chem. **976**, 153–160 (2011)